Biochemistry

Article

Cite This: Biochemistry XXXX, XXX, XXX−XXX

pubs.acs.org/biochemistry

Evolutionarily Conserved Allosteric Communication in Protein Tyrosine Phosphatases

Michael K. Hjortness,[†] Laura Riccardi,[‡] Akarawin Hongdusit,[†] Peter H. Zwart,[§] Banumathi Sankaran,[§] Marco De Vivo,[‡] and Jerome M. Fox*[,†]

[†]Department of Chemical and Biological Engineering, University of Colorado, 3415 Colorado Avenue, Boulder, Colorado 80303, United States

[‡]Laboratory of Molecular Modeling and Drug Discovery, Istituto Italiano di Tecnologia, Via Morego 30, 16163 Genova, Italy

[§]Molecular Biophysics and Integrated Bioimaging, Lawrence Berkeley National Laboratory, Berkeley, California 94720, United States

Supporting Information

ABSTRACT: Protein tyrosine phosphatases (PTPs) are an important class of regulatory enzymes that exhibit aberrant activities in a wide range of diseases. A detailed mapping of allosteric communication in these enzymes could, thus, reveal the structural basis of physiologically relevant—and, perhaps, therapeutically informative—perturbations (i.e., mutations, post-translational modifications, or binding events) that influence their catalytic states. This study combines detailed biophysical studies of protein tyrosine phosphatase 1B (PTP1B) with bioinformatic analyses of the PTP family to examine allosteric communication in this class of enzymes. Results of X-ray crystallography, molecular dynamics simulations, and sequence-based statistical analyses indicate that PTP1B possesses a broadly distributed allosteric network that is evolutionarily conserved across the PTP family, and findings from both kinetic studies and mutational analyses show that this network is functionally intact in sequence-diverse PTPs. The allosteric network resolved in this study reveals new sites for targeting allosteric inhibitors of PTPs and helps explain the functional influence of a diverse set of disease-associated mutations.

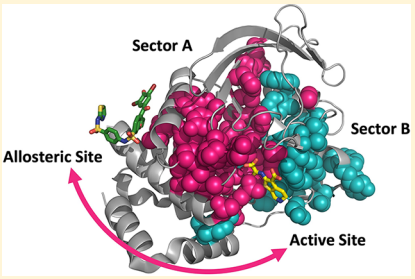

INTRODUCTION

The enzymatic phosphorylation of tyrosine residues is centrally important to cellular function and is anomalously regulated in an enormous range of diseases (e.g., diabetes, cancer, autoimmune disorders, and Noonan syndrome).[1−4] It is controlled by the concerted action of two classes of structurally flexible—and dynamically regulatable—enzymes: protein tyrosine kinases (PTKs), which catalyze the ATP-dependent phosphorylation of tyrosine residues, and protein tyrosine phosphatases (PTPs), which accelerate the hydrolytic dephosphorylation of phosphotyrosines.[5,6] A detailed understanding of the mechanisms by which these enzymes respond to activity-modulating structural perturbations (i.e., mutations, post-translational modifications, or binding events) could, thus, illuminate their contributions to various diseases and facilitate the design of new PTK- or PTP-targeted therapeutics.

Over the last several decades, many biophysical studies have dissected the catalytic mechanisms and regulatory functions of PTKs,[7,8] which are common targets of pharmaceuticals.[9] Detailed analyses of PTPs, by contrast, have lagged behind.[10] These enzymes represent an underdeveloped source of biomedical insight and therapeutic potential (no inhibitors of PTPs have cleared clinical trials).

Classical PTPs use two loops to dephosphorylate tyrosine residues. The P-loop (∼8 residues) binds phosphate moieties through a positively charged arginine, which enables nucleophilic attack by a nearby cysteine; the WPD loop (∼10 residues) contains a general acid catalyst (an aspartate) that protonates the tyrosine leaving group and hydrolyzes the phosphoenzyme intermediate.[11−13] During catalysis, the P-loop remains fixed, while the WPD loop moves ∼10 Å between open and closed states. Nuclear magnetic resonance (NMR) analyses suggest this movement controls the rate of catalysis.[14]

Recent analyses of protein tyrosine phosphatase 1B (PTP1B)—an important drug target for the treatment of diabetes, obesity, and breast cancer—indicate that motions of its WPD loop are regulated by an allosteric network that extends to its C-terminus (see Figure 1A).[15,16] This network is susceptible to modulation by both (i) inhibitors that displace its C-terminal α7 helix[17,18] and (ii) mutations that disrupt communication between the α7 helix and the WPD loop;[15] the specific collection of residues that enable allosteric communication in PTP1B—and, perhaps, other PTPs—however, has yet to be fully resolved.

This study combines biophysical, bioinformatic, and kinetic analyses to map the allosteric communication network of PTP1B and to assess the relevance of that network to other PTPs. This mapping has two goals: (i) the identification of allosteric sites that could supply new targets for selective

Received: June 16, 2018
Revised: September 20, 2018
Published: October 5, 2018

DOI: 10.1021/acs.biochem.8b00656
Biochemistry XXXX, XXX, XXX−XXX

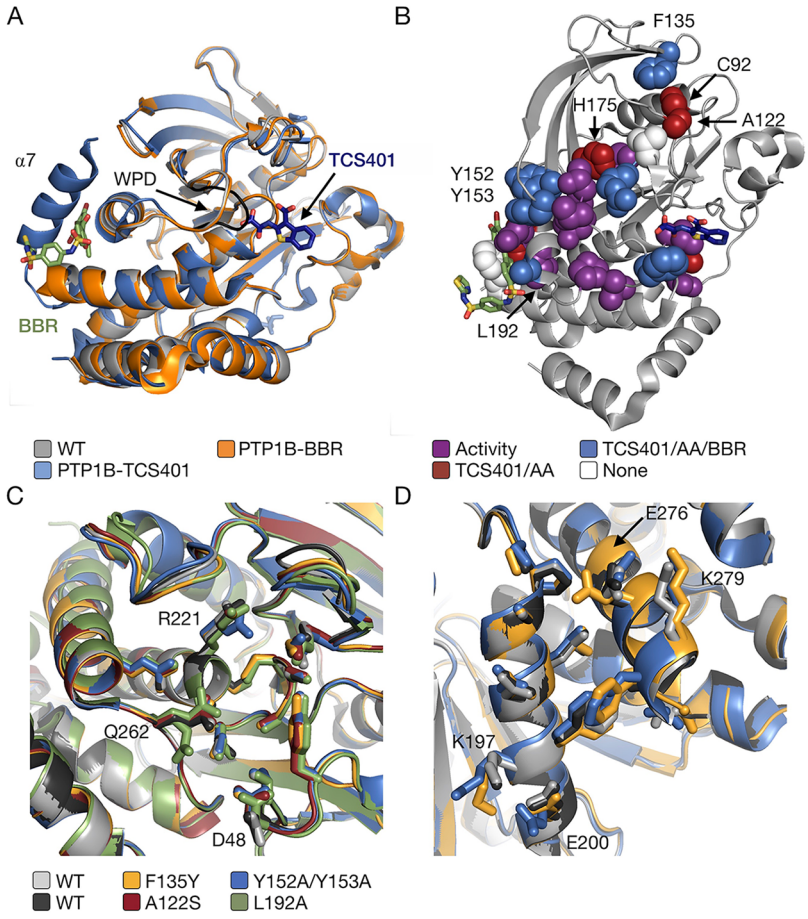

Figure 1. Analysis of mutations. (A) An alignment of apo (gray, PDB entry 3A5J), competitively inhibited (blue, 5K9W, TCS401), and allosterically inhibited (orange, 1T4J, BBR) crystal structures of PTP1B. Competitive inhibitors lock the WPD loop in a closed conformation (black) and stabilize the α7 helix; allosteric inhibitors displace the α7 helix and prevent the WPD loop from closing. (B) The apo structure of PTP1B shows the locations of mutations that (purple) alter the activity of the enzyme (i.e., change k_{cat} and/or K_m by 50% or more), (red) modify its sensitivity to inhibitors that bind to the active site (TCS401 and/or AA), (blue) modify its sensitivity to more than one variety of inhibitor (i.e., TCS401 or AA, which bind at the active site, *and* BBR, which binds at the allosteric site), and (white) exert no effect. (C, D) Alignments of crystal structures with mutations that are located outside of the active site [panel (C)] and/or the allosteric site [panel (D)], but that disrupt inhibition at those sites. Structures: wild-type (3A5J and 5K9V), F135Y (6CWU), A122S (6CWV), Y152A/Y153A (5KA2), and L192A (5KA8). [Note: These structures possess similar resolutions of 1.7−2.08 Å and space groups of $P3_121$ and $P3_221$.] Mutations do not cause major conformational changes in the backbone or side chains of the sites at which they influence inhibition.

allosteric modulators of PTPs (i.e., pharmaceutical leads) and (ii) the identification of structural features that help explain the functional influence of disruptive mutations.

EXPERIMENTAL SECTION

Materials. We purchased TCS401, or 2-[(carboxycarbonyl)-amino]-4,5,6,7-tetrahydro-thieno[2,3-*c*]pyridine-3-carboxylic acid hydrochloride, from Santa Cruz Biotechnology (Santa Cruz, CA); BBR, or 3-(3,5-dibromo-4-hydroxy-benzoyl)-2-ethyl-benzofuran-6-sulfonic acid-(4-(thiazol-2-ylsulfamyl)-phenyl)-amide, from Cayman Chemical (Ann Arbor, MI); and all other reagents from Sigma−Aldrich (St. Louis, MO).

Protein Expression and Purification. We overexpressed the catalytic domains $PTP1B_{1-321}$, $PTP1B_{1-281}$,TC-PTP_{1-292}, and $SHP2_{237-529}$ in BL21(DE3) competent *E. coli* cells (Thermo Fisher) via pET21b plasmids. Each plasmid contained a PTP gene fused to a C-terminal 6x polyhistidine tag. We followed methods for protein expression and protein purification detailed previously.[19]

Protein Crystallization and X-ray Crystallography. We prepared crystals of PTP1B by using hanging drop vapor diffusion. In brief, we performed the following steps: (i) We prepared a concentrated protein solution of PTP1B (~400 μM PTP1B, 50 mM HEPES, pH 7.3) and a crystallization solution (100 mM HEPES, 200 mM magnesium acetate, and 14% polyethylene glycol 8000, pH 7.5). (ii) We mixed 3 μL of the protein solution with 6 μL of the crystallization solution on the surface of a reservoir cover (EasyXtal CrystalSupport, Qiagen). (iii) We inverted the cover over a 2-mL reservoir filled with 1 mL of crystallization solution and incubated the setup at 4 °C.

We collected X-ray diffraction (XRD) data through the Collaborative Crystallography Program of the Berkeley Center for Structural Biology (Lawrence Berkeley National Lab), and we solved crystal structures with the following steps: (i) We performed integration, scaling, and merging of XRD data by using the xia2 software package.[20] (ii) We analyzed intensity statistics with Phenix.xtriage,[21] a program compatible with the Python-based Hierarchical Environment for Integrated Crystallography (Phenix).[22] (iii) We performed molecular replacement by using Phaser and 3A5J (PDB entry) as a search model.[23] (iv) We refined our structures with the phenix.refine graphical interface,[24] and we performed reciprocal space

DOI: 10.1021/acs.biochem.8b00656
Biochemistry XXXX, XXX, XXX−XXX

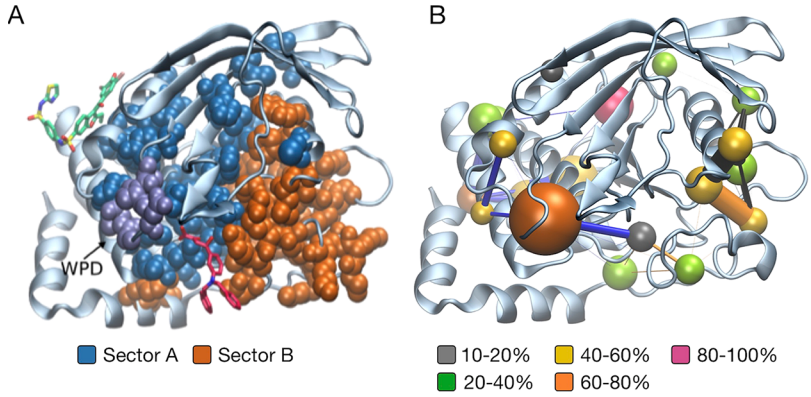

Figure 2. Evidence of an evolutionarily conserved allosteric network. (A) The results of a statistical coupling analysis. The orange and blue clusters represent two groups of residues, termed "sectors", that exhibit strong intragroup correlations in nonrandom distributions of amino acids. Highlights show the allosteric site (green inhibitor, PDB entry 1T4J), the active site (red inhibitor, 3EB1), and residues from sector A located within the WPD loop (purple spheres). (B) An analysis of crosstalk between pockets of PTP1B modeled with MD simulations. Pockets appear as spheres, colored according to their persistency along the MD trajectory; the size of each sphere indicates its average volume in MD simulations (all pockets are large enough to accommodate at least three molecules of water). Links have thicknesses proportional to the frequency of interpocket merging and splitting events (i.e., communication), and their colors indicate connections between pockets with residues from sector A (blue) or sector B (orange). Five connected pockets include residues from sector A, and five include residues from sector B; these groups of communicating pockets, which interconnect, support the allosteric functionality of sectors A and B.

refinement through several rounds of manual model adjustment in COOT,[25] followed by one round of PDB-REDO.[26] The crystallographic data collected in this study are reported in Table S2 of the Supporting Information.

Statistical Coupling Analysis (SCA). We performed a statistical coupling analysis of the PTP family by using approaches similar to those outlined previously:[27,28] (i) We used BLAST to search the nonredundant NCBI database for sequences similar to PTP1B (Uniprot P18031), and we aligned 3755 of those sequences—a number within the range (∼1000−5000) previously found to be sufficient for SCA[27,29]—with Clustal Omega (default settings). (ii) We removed sequence positions with a gap frequency of >20%, and we eliminated a single member of each pair with a sequence identity of >95%. These steps yielded a set of ∼700 sequence-distinct PTPs. (iii) We estimated the conservation of different positions in our alignment by using the Kullback−Leibler relative entropy to quantify the divergence between the distribution of amino acids observed at a specific position and the average distribution of amino acids observed in all proteins. (iv) We calculated conservation-weighted positional correlation and sequence correlation matrices, as described in the work of Halabi et al.[27] (v) We performed hierarchical clustering of the positional correlation matrix to identify groups of amino acids that displayed strong intragroup correlations (see Figure S1A in the Supporting Information). (vi) We performed an eigenvalue decomposition of the conservation-weighted positional correlation matrix. (vii) We used an independent component analysis to transform the top eight eigenvectors into eight maximally independent components. (viii) We performed a singular value decomposition of the sequence alignment to map the independent components of the positional correlation matrix onto sequence space. This analysis yielded no obvious connection between the groups of positionally correlated sites and groups in sequence space (see Figures S1B and S1C in the Supporting Information). (ix) We fit histograms of independent components of the positional correlation matrix to a *t*-distribution, and we used a 90% cutoff to select positions with the largest weights within each component. (x) The positions returned by two of the top independent components closely resembled the two groups of positions identified in our clustering analysis (i.e., sector A included 100% of the sites in the small cluster in Figure S1A in the Supporting Information, and sector B included 70% of those in the large cluster) and, when mapped onto the surface of PTP1B, defined sets of proximally positioned residues (see Figure 2A, as well as Figure S1D and Table S3A in the Supporting Information). Other (lower) independent components, which returned spatially diffuse sets of sites, may have interesting functional implications, but we did not explore them in this study.

Analysis of Interpocket Crosstalk. We examined dynamic crosstalk between surface pockets of PTP1B by using a molecular dynamics (MD) trajectory generated in our previous study.[19] In brief, we monitored the evolution of pockets on the surface of an apo form of PTP1B by using Pocketron.[30] This algorithm uses NanoShaper 0.7[31] to identify pockets of a defined size (e.g., a volume sufficient to accommodate three or five molecules of water), and it tracks the evolution of those pockets along an MD trajectory (snapshots every 150 ps). The temporal exchange of atoms between adjacent pockets provides a means of identifying hidden allosteric communication networks.[30] Figure 2B, as well as Figure S4 and Tables S3C and S3D in the Supporting Information show the results of this analysis.

Calculation of Sequence Identity. We calculated sequence identity between the catalytic domains of PTPs (i.e., $PTP1B_{1-321}$, $TC\text{-}PTP_{1-292}$, and $SHP2_{237-529}$) by using EMBOSS Needle.[32] The range of sequence identities reported in the main text correspond to the least similar pair (PTP1B and SHP2, 30%) and most similar pair (PTP1B and TC-PTP, 63%).

Enzyme Kinetics. We measured the kinetics of PTP-catalyzed hydrolysis of *p*-nitrophenyl phosphate (pNPP) by using a Spectramax M2 plate reader to monitor the formation of *p*-nitrophenol (absorbance at 405 nm) at intervals of 5 s. The composition of each reaction was as follows: PTP (0.05−0.1 μM), pNPP (0.17, 0.33, 0.67, 2, 5, 10, 15, and 20 mM), and buffer (50 mM HEPES, 2%−10% DMSO, 50 μg/mL BSA, pH 7.3). BBR, when present, was included at concentrations of 0, 10, 20, and 40 μM. Table S1B in the Supporting Information details discrete kinetic measurements.

DOI: 10.1021/acs.biochem.8b00656
Biochemistry XXXX, XXX, XXX−XXX

Statistical Analysis of Kinetic Models. We analyzed the inhibitory effect of BBR on various PTPs by evaluating four models of inhibition (see Figures S5 and S6 in the Supporting Information). For each kinetic dataset, we used an *F*-test to compare a two-parameter model of mixed inhibition to several single-parameter models, and we used Akaike's Information Criterion (AIC, or Δ_i) to compare the single-parameter models to each other. In Table S4 in the Supporting Information, mixed models with $p < 0.05$ are superior to all single-parameter models, and single-parameter models with $\Delta_i > 5$ are inferior to the reference "best-fit" model.

Estimation of IC_{50}. We estimated the half maximal inhibitory concentration (IC_{50}) of BBR by using kinetic models to estimate the concentration of inhibitor required to reduce initial rates of PTP-catalyzed hydrolysis of 20 mM of pNPP by 50%; we chose this high concentration of substrate, because it minimizes the concentration dependence of IC_{50} values. We used the MATLAB function "nlparci" to determine the confidence intervals of kinetic parameters, and we propagated those intervals to estimate corresponding confidence on IC_{50}.

Analysis of Mutations in PTPs. We assembled lists of previously studied mutations (i.e., functionally influential and/or disease-associated) by surveying the literature. We placed these mutations into two groups: Group 1 includes experimentally characterized mutations (Table S5A in the Supporting Information). For this group, we classified mutations as having a large influence on activity when they changed k_{cat}, K_m, or a defined activity by 50%, and we characterized them as having a significant influence on inhibition when their effect on K_d or inhibitor-modulated activity was large relative to other mutations in each study. Group 2 includes disease-associated mutations (i.e., both characterized and uncharacterized) identified in genetic analyses (Table S5B in the Supporting Information). For each group, we used PyMOL and PDB entry 3A5J to evaluate the number of residues in sectors A and B that are proximal (≤4 Å) to mutated residues (e.g., residue A for A122F).

Statistical Analysis of Distributions. We used the Kolmogorov−Smirnov statistical test to determine if multiple sample distributions belonged to the same parent distribution. In our first analysis, we compared distributions of the relative solvent accessible surface areas of residues in sectors A or B to a distribution of the relative solvent accessible surface areas of all residues in the catalytic domain (see Figure S2 in the Supporting Information). This analysis indicated that the distributions were different from each other ($P < 0.01$). In the second analysis, we assessed the positional bias of disease-associated mutations by comparing cumulative distributions describing (i) the proximity of mutations to network residues and (ii) the proximity of randomly selected sites to network residues. This analysis indicated that the two distributions were indistinguishable from each other ($P < 0.01$).

RESULTS AND DISCUSSION

Mutations Provide Evidence of a Broadly Distributed Allosteric Network. Two recent biophysical studies of PTP1B provide a starting point for mapping allosteric communication in this enzyme: (i) A systematic nuclear magnetic resonance (NMR) analysis of PTP1B dynamics identified several residues located outside of the active site that, when mutated, can disrupt catalytically essential motions of its WPD loop.[15] (ii) A detailed study of terpenoid-mediated inhibition showed that numerous mutations located outside of the active site and/or primary allosteric site can disrupt inhibition by molecules that bind to those sites.[19] Figure 1B consolidates the results of both studies and supplements them with newly collected activity data on mutants from the second (see Table S1 in the Supporting Information); the delocalized arrangement of functionally influential residues—some of which (e.g., C92A, A122S, A122F, H175A, and F135Y) are distal to regions of known allosteric relevance—suggests the presence of a broadly distributed allosteric network.

Distally Influential Mutations Do Not Affect the Backbone Conformation of PTP1B. X-ray crystallography provides a useful means of resolving structural changes that enable long-range communication in proteins.[33] To search for structural features that explain the delocalized influence of mutations in PTP1B, we aligned X-ray crystal structures of $PTP1B_{A122S}$ and $PTP1B_{F135Y}$ collected in this study with previously solved structures of $PTP1B_{Y152A/Y153A}$ and $PTP1B_{L192A}$. We chose these mutants for two reasons: (i) Their mutated residues are located outside of the regions at which they influence catalytic activity and/or inhibition and, thus, appear to participate in allosteric communication with those regions. (ii) Their mutated residues are distant from one another (i.e., A122 and F135 are located over 18 Å away from Y152 and Y153) and may, thus, represent spatially distinct entry points into an allosteric system (see Figure 1B). To our surprise, mutated residues did not alter the conformation of the protein backbone and caused negligible—and largely isolated—structural distortions in the side chains that line the active site or allosteric site (i.e., differences in the conformations of side chains in these sites are similar to their differences in alternative structures of the wild-type enzyme or appear in the absence of concerted changes in neighboring residues; see Figures 1C and 1D). Crystallographic results, thus, indicate that mutations do not affect catalysis or inhibition by triggering gross changes in protein conformation, but suggest a subtler—and, perhaps, dynamically focused—influence for which residue-specific contributions may be difficult to ascertain with structural methods alone.

PTPs Possess an Evolutionarily Conserved Allosteric Network. Statistical coupling analysis (SCA) provides an alternative means of resolving allosteric networks in proteins.[34] This method identifies correlations in nonrandom distributions of amino acids between different positions in a multiple sequence alignment; groups of positions with strong intragroup correlations—groups referred to as "sectors"—can reveal evolutionarily conserved functional domains (e.g., allosteric networks or binding interfaces).[27] To search for allosteric networks in PTP1B, we performed an SCA of ∼700 sequence-distinct members of the PTP family (i.e., sequences with <95% similarity; see Figure S1 in the Supporting Information). This analysis revealed two sectors that, when mapped onto the surface of PTP1B, define networks of proximally positioned residues. Sector A connects the C-terminal allosteric site to the WPD loop and includes numerous sites (e.g., R221, Pro185, Trp179, and Phe269) previously implicated in allosteric communication between these two regions.[35] Sector B connects the active site to several nearby loops with no previously established allosteric relevance (see Figure 2A, as well as Table S3A in the Supporting information). Sectors A and B, which are adjacent to each other, constitute ∼26% of the catalytic domain and contain disproportionately large fractions of buried residues (i.e., 80% and 72% of the residues in sectors A and B, respectively, have relative solvent accessible surface areas of 0−20%; only 48% of

DOI: 10.1021/acs.biochem.8b00656
Biochemistry XXXX, XXX, XXX−XXX

the full catalytic domain is similarly buried [see Figure S2 in the Supporting Information]). Interestingly, all influential mutations from Figure 1B are located near sectors A and B (≤4 Å, a distance sufficient to include hydrogen bonds and van der Waals interactions between polar and nonpolar residues, respectively[36]); nonconsequential mutations (i.e., V113Y and F280Y), by contrast, appear farther away (>5 Å; see Table S5 in the Supporting Information). The enhanced influence of mutations located near sectors A and B suggests that these two evolutionarily conserved sectors enable allosteric communication in PTPs.

The use of statistical analyses such as SCA to resolve allosteric systems is controversial. Several studies carried out with alternative approaches for examining residue−residue coevolution (notably, the GREMLIN pseudo-likelihood method[37] and direct-coupling analysis[38]) suggest that most coevolving residues are spatially proximal—an attribute inconsistent with long-range evolutionary coupling. We hypothesized that these alternative approaches, which exploit analytical frameworks that bias them toward pairs of contacting residues, should nonetheless reveal high densities of paired residues within conserved allosteric networks, provided those networks function through residue−residue contacts. We used the GREMLIN pseudo-likelihood approach to test this hypothesis.[37] As expected, our analysis identified interconnected networks of coevolving pairs located within sectors A and B (SI Note 1 and Figure S3, as well as Table S3B in the Supporting Information). The overlap between the evolutionarily constrained regions identified with SCA and GREMLIN is consistent with an evolutionarily conserved allosteric functionality.

We supplemented our bioinformatic analyses, which examine family-wide evolutionary trajectories, by using MD simulations to carry out a focused study of allosteric communication in PTP1B. Starting with an MD simulation of PTP1B in its apo form, we tracked the temporal exchange of atoms between pockets (i.e., clefts capable of accommodating three or more molecules of water), and we used the frequency of exchange events as a metric for interpocket connectivity. This approach has been used to identify hidden allosteric networks on the surfaces of proteins and, thus, allowed us to look for similar networks on the surface of PTP1B.[30] Our results revealed interconnected pockets located within sectors A and B (see Figure 2B, as well as Figure S4A and Table S3C in the Supporting Information); these pockets support the allosteric relevance of those sectors. Nonsector pockets and residues—some of which disappear with stricter thresholds for pocket size (Figure S4B in the Supporting Information)—are somewhat surprising, but likely reflect the tendency of conserved structural motifs to exhibit structural deviations across protein families (consider the binding pockets of cryptochromes[29]). More broadly, agreement between four complementary analyses—two sequence-based analyses, a mutational study, and a computational analysis—provides strong evidence that sectors A and B, which interconnect, define an evolutionarily conserved allosteric communication network.

The Allosteric Network Is Functionally Intact on Sequence-Diverse PTPs. The results of our sequence-based analyses are intriguing because they indicate that the allosteric control system found in PTP1B is broadly conserved across the PTP family. To test this finding, we examined the functional relevance of sector residues in T-cell protein tyrosine phosphatase (TC-PTP) and protein tyrosine phosphatase nonreceptor-type 11 (SHP2)—two enzymes that share 30%−63% sequence identity with PTP1B. First, we assessed the susceptibility of TC-PTP and SHP2 to BBR; this inhibitor binds to a weakly conserved site on PTP1B (see Figure 3A)

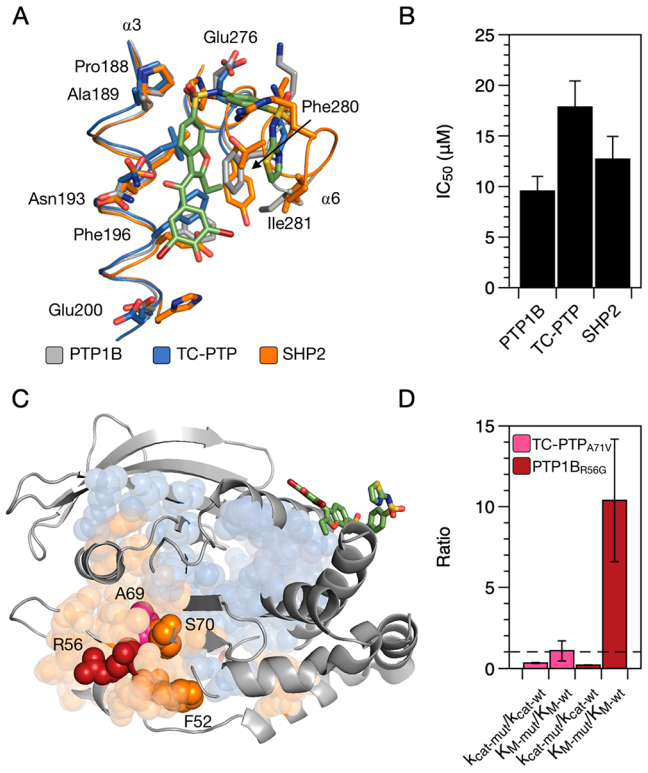

Figure 3. Analysis of allosteric susceptibility. (A) An alignment of crystal structures of PTP1B (PDB entry 1T4J), TC-PTP (1L8K), and SHP2 (3B7O) shows the binding site of BBR (green). The amino acids that line this site are labeled for PTP1B; they are weakly conserved between PTPs. (B) The susceptibility of TC-PTP and SHP2 to BBR-mediated inhibition suggests that these two enzymes possess the allosteric network through which BBR functions (i.e., residues included sector A). (C) A crystal structure of PTP1B (3A5J) highlights the locations of functionally influential mutations identified in sector B: A69V in PTP1B, and F285S/L, R289G, and N308D in SHP2 (i.e., F52, R56, and S70 in PTP1B). These mutations are located far (∼13−17 Å) from the active site (i.e., the bound position of TCS401 in aligned structures). Colors show sector A (transparent blue), sector B (transparent orange), and BBR (green). (D) Mutants $PTP1B_{R56G}$ and $TC\text{-}PTP_{A71V}$, analogues of the previously characterized SHP_{R289G} and $PTP1B_{A69V}$, exhibit reduced catalytic activities—a result suggestive of the conserved allosteric functionality of sector B in PTP1B, TC-PTP, and SHP2. The dashed line delineates a ratio of 1 between mutant and wild-type kinetic parameters. In panels (B) and (D), error bars represent 95% confidence intervals.

that allosterically modulates WPD loop dynamics through residues in sector A.[15,16] To our satisfaction, BBR could inhibit both enzymes and, thus, confirmed that these residues maintain their allosteric functionality in different PTPs (Figure 3B). The sensitivity of TC-PTP to BBR-mediated inhibition is consistent with its sensitivity to other allosteric inhibitors of PTP1B;[39] the sensitivity of SHP2 to this class of inhibitors, by contrast, has not been reported previously.

Next, we focused on sector B. This sector has no known binding sites, so we explored its functional relevance by searching the literature for activity-modulating mutations located within it. We found five: A69V in PTP1B, and F285S/L, R289G, and N308D in the full-length SHP2 (the latter set

DOI: 10.1021/acs.biochem.8b00656
Biochemistry XXXX, XXX, XXX−XXX

maps to F52, R56, and S70 in PTP1B; see Figure 3C).[40−43] All of these mutations are located far (∼13−17 Å) from the active site, and two—A69V and R289G—are not proximal (≤4 Å) to residues from sector A (see Figure 4C, as well as Figure S7 in the Supporting Information). To verify the functional relevance of these latter two mutations, we introduced them into PTP1B and TC-PTP (i.e., we generated $PTP1B_{R56A}$ and $TC\text{-}PTP_{A71V}$, which are analogues of $SHP2_{R289G}$ and $PTP1B_{A69V}$, respectively). Both mutations caused large changes in k_{cat} and/or K_M (i.e., they reduced k_{cat} or increased K_M by >50%; see Figure 3D). This effect on activity, when combined with previous mutational studies, suggests that the allosteric functionality of residues in sector B is conserved across PTP1B, TC-PTP, and SHP2.

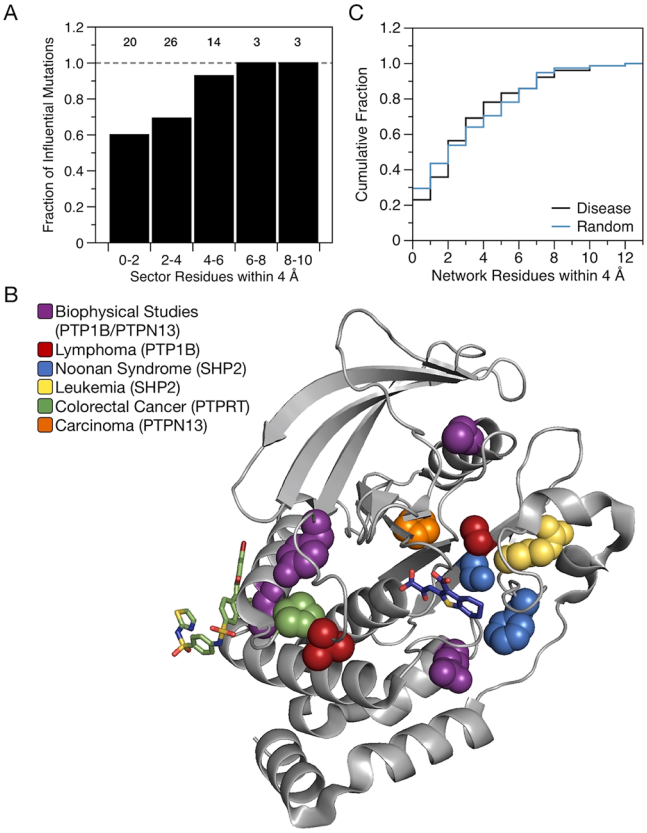

Figure 4. Analysis of pathologically relevant mutations. (A) This plot shows the influential fraction of experimentally characterized mutations grouped by their proximity to network residues. All mutations proximal (≤4 Å) to five or more network residues are "influential" (i.e., they altered k_{cat} or K_M by ≥50% or had a detectable influence on inhibition); nonconsequential mutations, by contrast, have fewer neighboring network residues. Sample sizes for each grouping appear at the top of the plot. (B) A crystal structure of PTP1B (gray, PDB entry 3A5J) highlights the locations of influential mutations at network residues; colors indicate whether they were introduced in biophysical studies or found in diseases. (C) Two cumulative distribution functions describe numbers of network residues proximal to (i) mutations identified in diseases and (ii) a random selection of sites. The two distributions are indistinguishable from each other (P < 0.01), suggesting that disease-associated mutations do not occur preferentially near the allosteric network.

Functionally Influential Mutations Tend To Occur Near the Allosteric Network. The contribution of PTPs to essential regulatory functions is underscored by the frequency with which they are mutated in diseases, particularly cancer.[40,44,45] To determine if previously studied mutations in PTPs (both those identified in diseases and those introduced in biochemical studies) influence function through allosteric modulation, we examined their proximity to sectors A and B. We focused on allosteric effects by limiting our analysis to mutations located outside of the core of the active site (i.e., residues within 5 Å of the competitive inhibitor TCS401 in PDB entry 5K9W). To begin, we grouped experimentally characterized mutations by their proximity to network residues (i.e., we counted the number of network residues within 4 Å of each mutated residue in PTP1B), and we calculated the fraction of those mutations that influence function. Figure 4A shows the results of this analysis. The fraction of functionally influential mutations increases with the number of neighboring network residues. In fact, all 14 previously identified mutations *at* network residues—many of which are found in diseases (see Figure 4B)—alter activity and/or susceptibility to inhibition. Importantly, analyses that grouped mutated sites by (i) their proximity to all residues (i.e., both sector and nonsector) or (ii) their solvent accessible surface area did not reveal obvious trends, and a more restrictive analysis that focused only on activity-modulating mutations (rather than mutations that influence *either* activity *or* susceptibility to inhibition) did not alter those trends (see Figure S8 in the Supporting Information). Our analysis thus suggests that many of the influential mutations identified in previous studies may function by modulating the allosteric network defined by sectors A and B.

To determine how the allosteric network affects the locations in which mutations tend to occur in diseases (an analysis distinct from our study of their functional influence), we compared the proximity of network residues to two sets of sites: (i) mutations identified in diseases and (ii) randomly selected sites. Surprisingly, proximity distributions were indistinguishable between these two sets (P < 0.01; see Figure 4C), suggesting a lack of positional bias in the location of naturally occurring mutations. This result is, perhaps, unsurprising, given the cancerous—and, thus, genetically diverse—origin of tabulated PTP mutations (i.e., cancer enables an efficient and largely random sampling of mutagenic sites); in light of Figure 4A, it may indicate that some natural mutations exhibit nonallosteric influences, such as effects on PTP stability, expression level, localization, substrate specificity, or capacity to engage in protein−protein interactions.

■ CONCLUSION

The results of this study suggest that all PTPs possess an evolutionarily conserved allosteric network that sensitizes them to structural perturbations at a broadly distributed set of sites. In brief, our statistical coupling analysis defines this network in two adjacent, evolutionarily conserved sectors; and MD simulations, inhibition studies, and mutational analyses show that residues within these sectors mediate allosteric communication with distal sites (e.g., the active site).

The allosteric functionality of sector residues has interesting implications for the sophisticated regulatory systems of PTPs. For SHP2, which has an SH2 domain that controls access to the active site,[46] results indicate that mutations in sector B may trigger conformational changes that affect catalytic activity, not just substrate access. This effect is consistent with both the conserved influence of R56 in PTP1B and SHP2 (i.e., only the latter of which has a regulatory domain) and previously reported kinetic studies and MD simulations of $SHP2_{N308D}$, a

DOI: 10.1021/acs.biochem.8b00656
Biochemistry XXXX, XXX, XXX−XXX

mutant that exhibits an enhanced catalytic activity in its activated state[42] (and, perhaps, a heightened propensity to transition into that state[47]). For PTP1B, in turn, our results suggest that the C-terminal α7-helix functions as a modulator—rather than a mediator—of allosteric communication. This effect is consistent with the absence of the α7-helix in the SCA-based sectors, the interpocket crosstalk that occurs without it, and the preserved susceptibility of an α7-less variant of PTP1B to inhibition by BBR (the IC_{50} of BBR is 29.1 ± 5.7 μM for $PTP1B_{1-281}$ and 9.6 ± 1.4 μM for the wild-type enzyme; see Figure S6 in the Supporting Information). Intriguingly, the functional independence of sectors A and B (if, in fact, such independence exists) may have interesting regulatory repercussions, but those repercussions are not clear from the present work.

The allosteric network also provides important guidance for drug design: (i) It motivates the development of allosteric inhibitors that bind to sites within sectors A and B; these sites are more structurally diverse than the active site[12] and could, thus, confer greater selectivity to PTP-targeted molecules. Previously identified variants of BBR that selectively inhibit PTP1B over TC-PTP highlight the value of one such site (i.e., the C-terminal allosteric site of PTP1B);[39] our results expand the relevance of this site to other PTPs, notably SHP2 (an immunomodulator targeted for the treatment of various types of cancer), and motivate the search for molecules that bind elsewhere within sectors A and B. (ii) It suggests potential mechanisms of drug resistance in genetically variable diseases, such as cancer. Allosterically influential mutations distributed across the surfaces of PTPs can enhance or reduce catalytic activity; in doing so, they might compensate for—or, perhaps, disrupt—the influence of PTP-targeted drugs. Of course, the regulatory domains of PTPs may further modulate—and, perhaps, affect binding to—the allosteric network mapped in this work.[12,48] The influence of these domains on allosteric control represents an important topic for future study.

Beyond PTPs, our findings have an important implication for the study of protein allostery. The consistency of bioinformatic results with three complementary analyses (e.g., a mutational analysis, a study of pocket crosstalk, and an analysis of inhibition) supports the controversial assertion that patterns of residue−residue coevolution can—at least within some classes of flexible and dynamically regulatable enzymes like PTPs—reveal the existence of functionally coupled groups of distally positioned amino acids (i.e., allosteric networks). The integration of these patterns into computational approaches for identifying cryptic allosteric sites (e.g., Markov state models[49,50]) could facilitate an assessment of the functional integrity of those sites across entire protein families or perhaps enable the identification of shared, catalytically essential structural features that enable—or otherwise rely on—long-range communication.

■ ASSOCIATED CONTENT

Supporting Information

The Supporting Information is available free of charge on the ACS Publications website at DOI: 10.1021/acs.biochem.8b00656.

A procedure for examining residue−residue-coevolution (i.e., the GREMLIN pseudolikelihood method) and detailed results of kinetic, bioinformatic, biostructural, and mutational analyses (PDF)

A spreadsheet showing discrete kinetic measurements of PTPs and mutants (XLSX)

A spreadsheet detailing analyses of experimentally characterized pathologically relevant mutations (XLSX)

A spreadsheet detailing analyses of disease-associated mutations (XLSX)

■ AUTHOR INFORMATION

Corresponding Author

*E-mail: jerome.fox@colorado.edu.

ORCID

Marco De Vivo: 0000-0003-4022-5661

Jerome M. Fox: 0000-0002-3739-1899

Notes

The authors declare no competing financial interest.

■ ACKNOWLEDGMENTS

This work was supported by funds provided by the University of Colorado, Boulder (M.K.H., A.H, and J.M.F., startup) and the National Science Foundation (Award No. 1750244 [for M.K.H. and J.M.F.] and Award No. 1804897 [for A.H.]). The ALS-ENABLE beamlines, which were used for X-ray crystallography, are supported in part by the NIH (Grant No. P30 GM124169-01). The Advanced Light Source is a Department of Energy Office of Science User Facility supported by Contract No. DE-AC02-05CH11231.

■ ABBREVIATIONS

PTP1B = protein tyrosine phosphatase 1B; TC-PTP = T-cell protein tyrosine phosphatase; SHP2 = protein tyrosine phosphatase nonreceptor type 11; BBR = 3-(3,5-dibromo-4-hydroxy-benzoyl)-2-ethyl-benzofuran-6-sulfonic acid-(4-(thiazol-2-ylsulfamyl)-phenyl)-amide; TCS401 = 2-[(carboxy-carbonyl)amino]-4,5,6,7-tetrahydro-thieno[2,3-*c*]pyridine-3-carboxylic acid hydrochloride; AA = abietic acid; SCA = statistical coupling analysis

■ REFERENCES

(1) Noble, M. E. M., Endicott, J. A., and Johnson, L. N. (2004) Protein kinase inhibitors: insights into drug design from structure. *Science 303*, 1800−1805.

(2) Chen, Y. N. P., Lamarche, M. J., Chan, H. M., Fekkes, P., Garcia-Fortanet, J., Acker, M. G., Antonakos, B., Chen, C. H. T., Chen, Z., Cooke, V. G., Dobson, J. R., Deng, Z., Fei, F., Firestone, B., Fodor, M., Fridrich, C., Gao, H., Grunenfelder, D., Hao, H. X., Jacob, J., Ho, S., Hsiao, K., Kang, Z. B., Karki, R., Kato, M., Larrow, J., La Bonte, L. R., Lenoir, F., Liu, G., Liu, S., Majumdar, D., Meyer, M. J., Palermo, M., Perez, L., Pu, M., Price, E., Quinn, C., Shakya, S., Shultz, M. D., Slisz, J., Venkatesan, K., Wang, P., Warmuth, M., Williams, S., Yang, G., Yuan, J., Zhang, J. H., Zhu, P., Ramsey, T., Keen, N. J., Sellers, W. R., Stams, T., and Fortin, P. D. (2016) Allosteric inhibition of SHP2 phosphatase inhibits cancers driven by receptor tyrosine kinases. *Nature 535*, 148−152.

(3) Rhee, I., and Veillette, A. (2012) Protein tyrosine phosphatases in lymphocyte activation and autoimmunity. *Nat. Immunol. 13*, 439−447.

(4) Rush, J., Moritz, A., Lee, K. A., Guo, A., Goss, V. L., Spek, E. J., Zhang, H., Zha, X. M., Polakiewicz, R. D., and Comb, M. J. (2005) Immunoaffinity profiling of tyrosine phosphorylation in cancer cells. *Nat. Biotechnol. 23*, 94−101.

(5) McClendon, C. L., Kornev, A. P., Gilson, M. K., and Taylor, S. S. (2014) Dynamic architecture of a protein kinase. *Proc. Natl. Acad. Sci. U. S. A. 111*, E4623−E4631.

(6) Den Hertog, J., Groen, A., and Van Der Wijk, T. (2005) Redox regulation of protein-tyrosine phosphatases. *Arch. Biochem. Biophys. 434*, 11−15.

DOI: 10.1021/acs.biochem.8b00656
Biochemistry XXXX, XXX, XXX−XXX

(7) Hubbard, S. R., and Till, J. H. (2000) Protein Tyrosine Kinase Structure and Function. *Annu. Rev. Biochem. 69*, 373−398.
(8) Lemmon, M. A., and Schlessinger, J. (2010) Cell signaling by receptor tyrosine kinases. *Cell 141*, 1117−1134.
(9) Wu, P., Nielsen, T. E., and Clausen, M. H. (2015) FDA-approved small-molecule kinase inhibitors. *Trends Pharmacol. Sci. 36*, 422−439.
(10) Yu, Z.-H., and Zhang, Z.-Y. (2018) Regulatory Mechanisms and Novel Therapeutic Targeting Strategies for Protein Tyrosine Phosphatases. *Chem. Rev. 118*, 1069−1091.
(11) Tautz, L., Critton, D. A., and Grotegut, S. (2013) Protein Tyrosine Phosphatases: Structure, Function and Implication in Human Disease. *Methods Mol. Biol. 1053*, 179−221.
(12) Barr, A. J., Ugochukwu, E., Lee, W. H., King, O. N. F., Filippakopoulos, P., Alfano, I., Savitsky, P., Burgess-Brown, N. A., Müller, S., and Knapp, S. (2009) Large-Scale Structural Analysis of the Classical Human Protein Tyrosine Phosphatome. *Cell 136*, 352−363.
(13) Jia, Z., Barford, D., Flint, A., and Tonks, N. (1995) Structural basis for phosphotyrosine peptide recognition by protein tyrosine phosphatase 1B. *Science 268*, 1754−1758.
(14) Whittier, S. K., Hengge, A. C., and Loria, J. P. (2013) Conformational Motions Regulate Phosphoryl Transfer in Related Protein Tyrosine Phosphatases. *Science 341*, 899−903.
(15) Choy, M. S., Li, Y., Machado, L. E. S. F., Kunze, M. B. A., Connors, C. R., Wei, X., Lindorff-Larsen, K., Page, R., and Peti, W. (2017) Conformational Rigidity and Protein Dynamics at Distinct Timescales Regulate PTP1B Activity and Allostery. *Mol. Cell 65*, 644−658.
(16) Li, S., Zhang, J., Lu, S., Huang, W., Geng, L., Shen, Q., and Zhang, J. (2014) The Mechanism of allosteric inhibition of protein tyrosine phosphatase 1B. *PLoS One 9*, e97668.
(17) Wiesmann, C., Barr, K. J., Kung, J., Zhu, J., Erlanson, D. A., Shen, W., Fahr, B. J., Zhong, M., Taylor, L., Randal, M., McDowell, R. S., and Hansen, S. K. (2004) Allosteric inhibition of protein tyrosine phosphatase 1B. *Nat. Struct. Mol. Biol. 11*, 730−7.
(18) Krishnan, N., Koveal, D., Miller, D. H., Xue, B., Akshinthala, S. D., Kragelj, J., Jensen, M. R., Gauss, C.-M., Page, R., Blackledge, M., Muthuswamy, S. K., Peti, W., and Tonks, N. K. (2014) Targeting the disordered C terminus of PTP1B with an allosteric inhibitor. *Nat. Chem. Biol. 10*, 558−566.
(19) Hjortness, M. K., Riccardi, L., Hongdusit, A., Ruppe, A., Zhao, M., Kim, E. Y., Zwart, P. H., Sankaran, B., Arthanari, H., Sousa, M. C., De Vivo, M., and Fox, J. M. (2018) Abietane-Type Diterpenoids Inhibit Protein Tyrosine Phosphatases by Stabilizing an Inactive Enzyme Conformation. *Biochemistry 57*, 5886.
(20) Winter, G. (2010) Xia2: An expert system for macromolecular crystallography data reduction. *J. Appl. Crystallogr. 43*, 186−190.
(21) Zwart, P. H., Grosse-Kunstleve, R. W., and Adams, P. D. (2005) Xtriage and Fest: automatic assessment of X-ray data and substructure structure factor estimation. *CCP4 Newsl. 43*, 27−35.
(22) Adams, P. D., Afonine, P. V., Bunkóczi, G., Chen, V. B., Davis, I. W., Echols, N., Headd, J. J., Hung, L. W., Kapral, G. J., Grosse-Kunstleve, R. W., McCoy, A. J., Moriarty, N. W., Oeffner, R., Read, R. J., Richardson, D. C., Richardson, J. S., Terwilliger, T. C., and Zwart, P. H. (2010) PHENIX: A comprehensive Python-based system for macromolecular structure solution. *Acta Crystallogr., Sect. D: Biol. Crystallogr. 66*, 213−221.
(23) McCoy, A. J., Grosse-Kunstleve, R. W., Adams, P. D., Winn, M. D., Storoni, L. C., and Read, R. J. (2007) Phaser crystallographic software. *J. Appl. Crystallogr. 40*, 658−674.
(24) Afonine, P. V., Grosse-Kunstleve, R. W., Echols, N., Headd, J. J., Moriarty, N. W., Mustyakimov, M., Terwilliger, T. C., Urzhumtsev, A., Zwart, P. H., and Adams, P. D. (2012) Towards automated crystallographic structure refinement with phenix.refine. *Acta Crystallogr., Sect. D: Biol. Crystallogr. 68*, 352−67.
(25) Emsley, P., and Cowtan, K. (2004) Coot: Model-building tools for molecular graphics. *Acta Crystallogr., Sect. D: Biol. Crystallogr. 60*, 2126−2132.
(26) Joosten, R. P., Long, F., Murshudov, G. N., and Perrakis, A. (2014) The *PDB_REDO* server for macromolecular structure model optimization. *IUCrJ 1*, 213−220.
(27) Halabi, N., Rivoire, O., Leibler, S., and Ranganathan, R. (2009) Protein Sectors: Evolutionary Units of Three-Dimensional Structure. *Cell 138*, 774−786.
(28) Raman, A. S., White, K. I., and Ranganathan, R. (2016) Origins of Allostery and Evolvability in Proteins: A Case Study. *Cell 166*, 468−481.
(29) Rosensweig, C., Reynolds, K. A., Gao, P., Laothamatas, I., Shan, Y., Ranganathan, R., Takahashi, J. S., and Green, C. B. (2018) An evolutionary hotspot defines functional differences between CRYPTOCHROMES. *Nat. Commun. 9*, 1138.
(30) La Sala, G., Decherchi, S., De Vivo, M., and Rocchia, W. (2017) Allosteric Communication Networks in Proteins Revealed through Pocket Crosstalk Analysis. *ACS Cent. Sci. 3*, 949.
(31) Decherchi, S., and Rocchia, W. (2013) A general and robust ray-casting-based algorithm for triangulating surfaces at the nanoscale. *PLoS One 8*, e59744.
(32) Rice, P., Longden, L., and Bleasby, A. (2000) EMBOSS: The European Molecular Biology Open Software Suite. *Trends Genet. 16*, 276−277.
(33) Van Den Bedem, H., Bhabha, G., Yang, K., Wright, P. E., and Fraser, J. S. (2013) Automated identification of functional dynamic contact networks from X-ray crystallography. *Nat. Methods 10*, 896−902.
(34) Süel, G. M., Lockless, S. W., Wall, M. A., and Ranganathan, R. (2003) Evolutionarily conserved networks of residues mediate allosteric communication in proteins. *Nat. Struct. Biol. 10*, 59−69.
(35) Keedy, D. A., Hill, Z. B., Biel, J. T., Kang, E., Rettenmaier, T. J., Brandao-Neto, J., Pearce, N. M., von Delft, F., Wells, J. A., and Fraser, J. S. (2018) An expanded allosteric network in PTP1B by multitemperature crystallography, fragment screening, and covalent tethering. *eLife 7*, e36307.
(36) Anishchenko, I., Ovchinnikov, S., Kamisetty, H., and Baker, D. (2017) Origins of coevolution between residues distant in protein 3D structures. *Proc. Natl. Acad. Sci. U. S. A. 114*, 9122.
(37) Kamisetty, H., Ovchinnikov, S., and Baker, D. (2013) Assessing the utility of coevolution-based residue-residue contact predictions in a sequence- and structure-rich era. *Proc. Natl. Acad. Sci. U. S. A. 110*, 15674−15679.
(38) Morcos, F., Pagnani, A., Lunt, B., Bertolino, A., Marks, D. S., Sander, C., Zecchina, R., Onuchic, J. N., Hwa, T., and Weigt, M. (2011) Direct-coupling analysis of residue coevolution captures native contacts across many protein families. *Proc. Natl. Acad. Sci. U. S. A. 108*, E1293−E1301.
(39) Wiesmann, C., Barr, K. J., Kung, J., Zhu, J., Erlanson, D. A., Shen, W., Fahr, B. J., Zhong, M., Taylor, L., Randal, M., McDowell, R. S., and Hansen, S. K. (2004) Allosteric inhibition of protein tyrosine phosphatase 1B. *Nat. Struct. Mol. Biol. 11*, 730−737.
(40) Gunawardana, J., Chan, F. C., Telenius, A., Woolcock, B., Kridel, R., Tan, K. L., Ben-Neriah, S., Mottok, A., Lim, R. S., Boyle, M., Rogic, S., Rimsza, L. M., Guiter, C., Leroy, K., Gaulard, P., Haioun, C., Marra, M. A., Savage, K. J., Connors, J. M., Shah, S. P., Gascoyne, R. D., and Steidl, C. (2014) Recurrent somatic mutations of PTPN1 in primary mediastinal B cell lymphoma and Hodgkin lymphoma. *Nat. Genet. 46*, 329−335.
(41) Bentires-Alj, M., Paez, J. G., David, F. S., Keilhack, H., Halmos, B., Naoki, K., Maris, J. M., Richardson, A., Bardelli, A., Sugarbaker, D. J., Richards, W. G., Du, J., Girard, L., Minna, J. D., Loh, M. L., Fisher, D. E., Velculescu, V. E., Vogelstein, B., Meyerson, M., Sellers, W. R., and Neel, B. G. (2004) Activating mutations of the Noonan syndrome-associated SHP2/PTPN11 gene in human solid tumors and adult acute myelogenous leukemia. *Cancer Res. 64*, 8816−8820.
(42) Keilhack, H., David, F. S., McGregor, M., Cantley, L. C., and Neel, B. G. (2005) Diverse biochemical properties of Shp2 mutants: Implications for disease phenotypes. *J. Biol. Chem. 280*, 30984−30993.
(43) LaRochelle, J. R., Fodor, M., Xu, X., Durzynska, I., Fan, L., Stams, T., Chan, H. M., LaMarche, M. J., Chopra, R., Wang, P.,

DOI: 10.1021/acs.biochem.8b00656
Biochemistry XXXX, XXX, XXX−XXX

Fortin, P. D., Acker, M. G., and Blacklow, S. C. (2016) Structural and Functional Consequences of Three Cancer-Associated Mutations of the Oncogenic Phosphatase SHP2. *Biochemistry 55*, 2269−2277.
(44) Tartaglia, M., Mehler, E. L., Goldberg, R., Zampino, G., Brunner, H. G., Kremer, H., Van der Burgt, I., Crosby, A. H., Ion, A., Jeffery, S., Kalidas, K., Patton, M. A., Kucherlapati, R. S., and Gelb, B. D. (2001) Mutations in PTPN11, encoding the protein tyrosine phosphatase SHP-2, cause Noonan syndrome. *Nat. Genet. 29*, 465−468.
(45) Östman, A., Hellberg, C., and Böhmer, F. D. (2006) Protein-tyrosine phosphatases and cancer. *Nat. Rev. Cancer 6*, 307.
(46) Barford, D., and Neel, B. G. (1998) Revealing mechanisms for SH2 domain mediated regulation of the protein tyrosine phosphatase SHP-2. *Structure 6*, 249.
(47) Darian, E., Guvench, O., Yu, B., Qu, C. K., and Mackerell, A. D. (2011) Structural mechanism associated with domain opening in gain-of-function mutations in SHP2 phosphatase. *Proteins: Struct., Funct., Genet. 79*, 1573.
(48) Chen, Y.-N. P., LaMarche, M. J., Chan, H. M., Fekkes, P., Garcia-Fortanet, J., Acker, M. G., Antonakos, B., Chen, C. H.-T., Chen, Z., Cooke, V. G., Dobson, J. R., Deng, Z., Fei, F., Firestone, B., Fodor, M., Fridrich, C., Gao, H., Grunenfelder, D., Hao, H.-X., Jacob, J., Ho, S., Hsiao, K., Kang, Z. B., Karki, R., Kato, M., Larrow, J., La Bonte, L. R., Lenoir, F., Liu, G., Liu, S., Majumdar, D., Meyer, M. J., Palermo, M., Perez, L., Pu, M., Price, E., Quinn, C., Shakya, S., Shultz, M. D., Slisz, J., Venkatesan, K., Wang, P., Warmuth, M., Williams, S., Yang, G., Yuan, J., Zhang, J.-H., Zhu, P., Ramsey, T., Keen, N. J., Sellers, W. R., Stams, T., and Fortin, P. D. (2016) Allosteric inhibition of SHP2 phosphatase inhibits cancers driven by receptor tyrosine kinases. *Nature 535*, 148−52.
(49) Bowman, G. R., Bolin, E. R., Hart, K. M., Maguire, B. C., and Marqusee, S. (2015) Discovery of multiple hidden allosteric sites by combining Markov state models and experiments. *Proc. Natl. Acad. Sci. U. S. A. 112*, 2734−2739.
(50) Bowman, G. R., and Geissler, P. L. (2012) Equilibrium fluctuations of a single folded protein reveal a multitude of potential cryptic allosteric sites. *Proc. Natl. Acad. Sci. U. S. A. 109*, 11681−11686.

■ NOTE ADDED AFTER ASAP PUBLICATION

This paper published ASAP on 10/26/2018. Figure 3 was corrected and the revised version was reposted on 10/30/2018.

DOI: 10.1021/acs.biochem.8b00656
Biochemistry XXXX, XXX, XXX−XXX